Insights on HIV-1 Tat:P/CAF bromodomain molecular recognition from in vivo experiments and molecular dynamics simulations

ARTICLE *in* PROTEINS STRUCTURE FUNCTION AND BIOINFORMATICS · MARCH 2005

Impact Factor: 2.63 · DOI: 10.1002/prot.20805 · Source: PubMed

9 AUTHORS, INCLUDING:

Sergio Pantano
Institut Pasteur de Montevideo
56 PUBLICATIONS **947** CITATIONS
SEE PROFILE

A. Ferrari
ETH Zurich
59 PUBLICATIONS **1,474** CITATIONS
SEE PROFILE

Daniele Gaudiosi
Horizon Discovery
2 PUBLICATIONS **271** CITATIONS
SEE PROFILE

Paolo Carloni
Forschungszentrum Jülich
276 PUBLICATIONS **5,974** CITATIONS
SEE PROFILE

Insights on HIV-1 Tat:P/CAF Bromodomain Molecular Recognition From In Vivo Experiments and Molecular Dynamics Simulations

Sergio Pantano,[1–3]† Alessandro Marcello,[4,5]† Aldo Ferrari,[5,7] Daniele Gaudiosi,[4]‡ Arianna Sabò,[6] Vittorio Pellegrini,[5] Fabio Beltram,[6] Mauro Giacca,[4,5]* and Paolo Carloni[1]*

[1]*International School for Advanced Studies (ISAS) and INFM-DEMOCRITOS Modeling Center for Research in Atomistic Simulation, Trieste, Italy*
[2]*IMASL, CONICET, National University of San Luis, San Luis, Argentina*
[3]*Venetian Institute of Molecular Medicine (VIMM), Padua, Italy*
[4]*Molecular Virology Laboratory, International Centre for Genetic Engineering and Biotechnology (ICGEB), Trieste, Italy*
[5]*National Enterprise for nanoScience and nanoTechnology—Istituto Nazionale di Fisica della Materia (NEST-CNR-INFM) and Scuola Normale Superiore, Pisa, Italy*
[6]*Molecular Medicine Laboratory, International Centre for Genetic Engineering and Biotechnology (ICGEB), Trieste, Italy*
[7]*Institut f. Biochemie Schafmattstr. 18 ETH Hönggerberg, CH-8093, Zürich*

ABSTRACT **Structural and functional studies indicate that, through its bromodomain, the cellular acetyltransferase P/CAF binds the acetylated Tat protein of human immunodeficiency virus type 1 (HIV-1) and promotes transcriptional activation of the integrated provirus. Based on the NMR structure of P/CAF complexed with an acetylated Tat peptide, here we use molecular dynamics simulations to construct a model describing the interaction between full length Tat and the P/CAF bromodomain. Our calculations show that the protein–protein interface involves hydrophobic interactions between the P/CAF ZA loop and the Tat core domain. In particular, tyrosines 760 and 761 of P/CAF, two residues that are highly conserved in most known bromodomains, play an essential role for the binding. Fluorescence resonance energy transfer (FRET) experiments performed in this work demonstrate that P/CAF proteins in which these tyrosines are mutated into hydrophilic residues neither bind to Tat inside the cells nor mediate Tat transactivation. The combination of theoretical and in vivo studies provides new insights into the specificity of bromodomain recognition. Proteins 2006;62:1062–1073.**

Key words: bromodomain/HIV-1 Tat; lysine acetylation; protein–protein interactions

INTRODUCTION

Regulation of human immunodeficiency virus type 1 (HIV-1) gene expression by the viral Tat *trans*-activator is a critical step in the viral life cycle. Tat is a small polypeptide that binds a *cis*-acting RNA element (*trans*-activation-responsive region, TAR) present at the 5′ ends of all viral messenger RNAs (mRNAs).[1,2] Through this interaction, Tat activates transcription from the HIV long terminal repeat (LTR) promoter by at least two different molecular mechanisms, both of which are mediated by its binding to several cellular proteins (for a comprehensive review, see Marcello et al.[3] and Karn[4]). The first mechanism involves the interaction of Tat with human Cyclin T1,[5] the cyclin subunit of CDK9 in the positive transcription elongation factor b (P-TEFb). This kinase complex phosphorylates the carboxy-terminal domain (CTD) of RNA Pol II, a molecular event associated with increased transcriptional processivity.[6] The second mechanism of Tat-induced transcriptional activation entails the recruitment of cellular proteins with histone acetyltransferase (HAT) activity, which relieves the inhibition that chromatin conformation imposes onto the HIV promoter.[7,8] These factors include the transcriptional coactivators p300 and the highly homologous cyclic adenosine monophosphate (cAMP)-responsive binding protein (CREB)-binding protein (CBP),[9] the p300/CBP-associated factor (P/CAF),[10] the general control nonderepressible-5 (GCN5) factor,[11] the TIP60 protein,[12] and the general transcription factor

The Supplementary Material referred to in this article can be found online at http://www.interscience.wiley.com/spages/0887-3585/suppmat/

Grant sponsor: National Research Program on AIDS of the Istituto Superiore di Sanità (to M. Giacca and A. Marcello). Grant sponsor: Fondo Investimenti per la Ricerca di Base of the Ministero dell'Istruzione, Università e Ricerca (FIRB-MIUR; to A. Marcello and M. Giacca). Grant sponsor: Human Frontier Science Program (HFSP; to A. Marcello and V. Pellegrini). Grant sponsor: National Institute for the Physics of Matter (INFM; to F. Beltram, V. Pellegrini, S. Pantano, and P. Carloni). Grant sponsor: Regione Autonoma Friuli Venezia Giulia (to S. Pantano and P. Carloni). Grant sponsor: Fondazione Cariparo (to S. Pantano). Grant sponsor: EC STREP; Grant number: 012182 (to A. Marcello).

*Correspondence to: Mauro Giacca, Director, ICGEB Trieste, Padriciano 99, 34012 Trieste, Italy. E-mail: giacca@icgeb.org and Paolo Carloni, International School for Advanced Studies, Via Beirut 4, 34014 Trieste, Italy. E-mail: carloni@sissa.it

†Both authors are to be considered as first author.

‡Current address: Istituto Europeo di Oncologia (IEO), Via Ripamonti 435, 20141 Milano, Italy

Received 17 January 2005; Revised 4 August 2005; Accepted 29 August 2005

Published online 16 December 2005 in Wiley InterScience (www.interscience.wiley.com). DOI: 10.1002/prot.20805

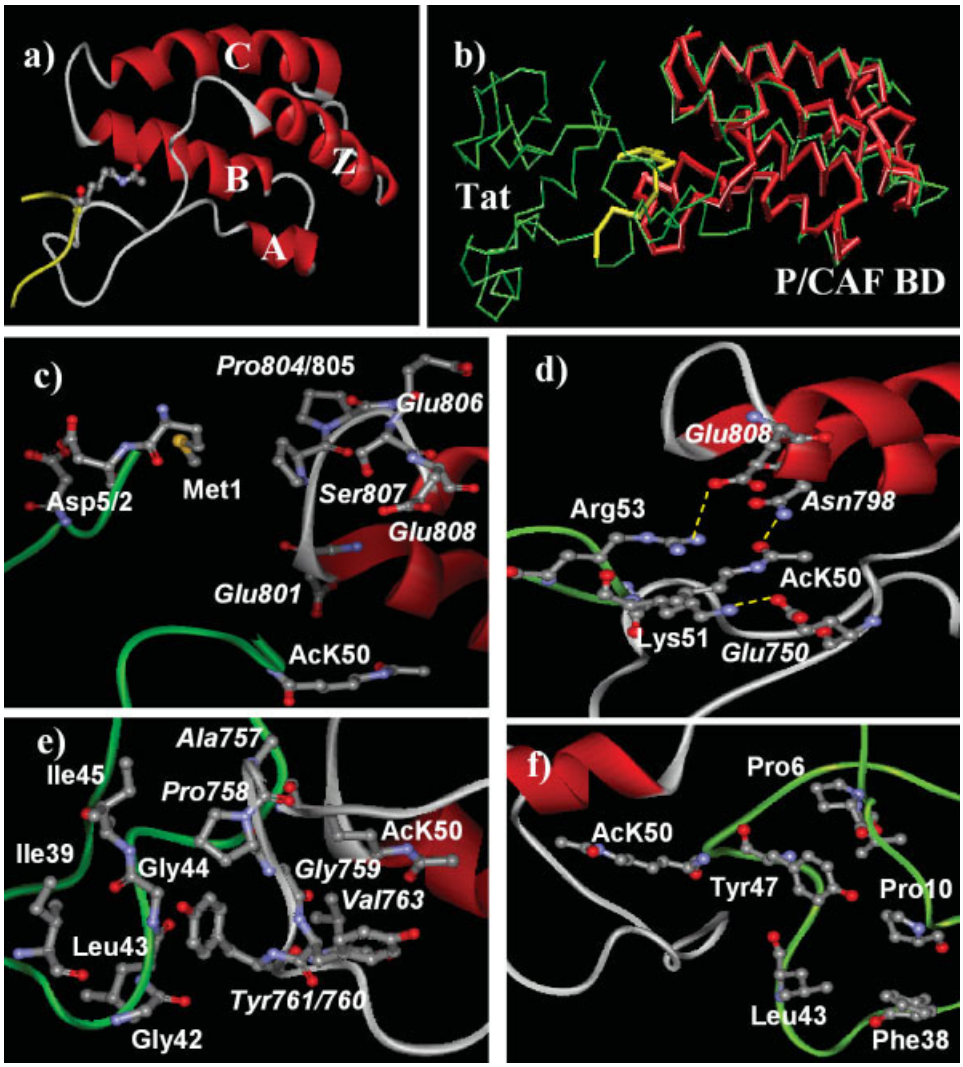

Fig. 1. AcK50 Tat:P/CAF BD interactions. (**a**) The NMR complex between P/CAF BD and AcK50 Tat peptide SYGRAcK$_{50}$KRRQRC (yellow).[21] For the sake of clarity, the only side-chain shown is that of Tat peptide AcK50. The labeling of the four helices of the BD is indicated. (**b**) Comparison between the NMR structure and the full P/CAF BD (red) and AcK50 Tat (green) as obtained with the final MD structure. Only the Cα atoms are shown. (**c**) Hydrophobic contacts between the N-terminal domain of Tat and the BC loop of P/CAF BD. The acidic residues that putatively limit a higher interaction surface are also shown. (**d**) Representation of the two salt bridges and the H-bond interaction between AcK50 and Asn798 conserved along different BDs. (**e**) Hydrophobic contacts between the Tat core domain–Tyr761 and AcK50–Tyr760. (**f**) position of Tyr47 within the protein–protein interface and its interactions with other Tat hydrophobic residues. The side-chain of AcK50 shown in (c) to (f) is to be used as a reference.

TAFII250.[13] Tat-recruited HATs acetylate histones in the LTR-proximal nucleosomes to activate transcription.[14] Besides histones, Tat itself is a substrate for acetylation by p300/CBP, P/CAF, and GCN5.[11,15–17] Tat is acetylated by P/CAF on Lys28 and by p300 and hGCN5 on Lys50. The acetylation of Tat has been proposed to regulate two discrete and functionally critical steps in transcription, binding to P-TEFb and the release of Tat from TAR RNA.[18–20]

Structural insights into the binding mode of P/CAF to acetylated Tat were provided by determination of the NMR structure of the peptide SYGRAcK$_{50}$KRRQRC (that corresponds to the Tat residues 46 to 55, with an acetyl group on lysine 50) in complex with the acetylated lysine (AcK)-binding domain of P/CAF[21] (Fig. 1). P/CAF consists essentially of two domains, a catalytic domain with histone acetyltransferase activity, which does not play any role in Tat binding, and an AcK-binding domain, termed the bromodomain (BD).[22] The P/CAF BD adopts a left-handed, four-helix bundle (helices α_Z, α_A, α_B, and α_C; Fig. 1) with a short loop linking helices α_B and α_C (BC loop) and a larger loop linking helices α_Z and α_A (ZA loop). This topology provides a rigid scaffold (the bundle) and a flexible part (ZA loop) that can adapt to the ligand shape.[23]

The relatively small association constant estimated for the P/CAF BD:AcK50 Tat peptide complex ($K_D \sim 10\ \mu M$)[21]

suggests that important interactions may arise by additional contacts present only in the full-length Tat protein. Starting from this BD/peptide structure, here we use molecular dynamics (MD) simulation techniques to construct and relax a model of the full-length AcK50 Tat:P/CAF BD interaction, and provide a functional validation of this model inside the cells. Owing to the intrinsic limitations of the theoretical approach, our model must not be considered as an atomic-detail structure; nevertheless, we found that, in addition to most of the interface contacts found in the NMR structure, a large part of the protein–protein interaction surface is formed by hydrophobic contacts between the core domain of Tat and the ZA loop of P/CAF. In particular, two tyrosine residues are predicted to play a crucial role in Tat binding: Y760, which interacts with AcK50 Tat, and Y761, which forms hydrophobic contacts with the Tat core domain. Consistent with this prediction, the mutation of these tyrosines to aspartic acids abolishes the coactivator potential of P/CAF on Tat transactivation and the physical association between the two proteins in living cells.

METHODS

Computational Details

Our calculations were based on the following:

1. The family of NMR structures of P/CAF BD in complex with the acetylated SYGRAcK$_{50}$KRRQC peptide [Protein Data Bank (PDB) entry: 1JM4 [21]]. Since no average structure was deposited, we selected model 13, which possesses the lowest pairwise root-mean-square deviation (RMSD) between the 25 models reported. The ionization states of the residues were those assumed in the NMR structure.
2. A structure of AcK50 Tat in aqueous solution, as obtained from a 3-ns MD simulation[24] obtained from the NMR structure of 86-residues-long Tat Z2 variant[25] based on the AMBER force field.

This force field has been shown to very accurately describe nucleic acid–binding proteins,[26] and in particular Tat.[27] We selected the MD snapshot with the lowest RMSD (0.6 Å) between the atoms of the backbone of the segment YGRAcK$_{50}$KRRQ in the peptide in complex with P/CAF and the corresponding residues in the full length AcK50 Tat protein.

The protein–protein complex model was built by fitting residues 47 to 54 onto the peptide. After fitting, the peptide molecule was removed. This procedure generated a number of close contacts at the protein–protein interface (see Supplementary Table 1) that were relaxed by energy minimization and MD simulations.

The complex was immersed in a simulation box containing ~11,000 water molecules and 15 neutralizing Cl^- counterions.[28]

MD calculations were carried out with the SANDER module of AMBER 6.0 suite of programs. Periodic rectangular boundary conditions were used. The particle mesh Ewald summation method[29] was used for long-range electrostatic interactions. A 10 Å cutoff was adopted for short-range nonbonded interactions. A dielectric constant of 1 was assumed. All chemical bonds were constrained using the SHAKE algorithm.[30] A timestep of 1 fs was used. Temperature and pressure were kept constant at 300 K and 1atm, respectively, by coupling the system to external baths[31] with coupling constants of $\tau_t = 0.05$ ps and $\tau_p = 0.5$ ps, respectively. For the protein and the counterions, the AMBER[32] force field parameters were used, respectively. For water, the transferable intermolecular potential (TIP3P) model[33] was chosen.

The Tat:P/CAF wild-type complex was relaxed with the following protocol:

1. Use of energy minimization with harmonic constraints on the backbone atoms of residues 47 to 54 and on all heavy atoms of AcK50 (see Supplementary Table 2). This relaxation removed all the bad contacts between the two proteins.
2. Use of a 0.03-ns MD simulation of the solvent and the counterions.
3. Six MD simulation steps, each lasting 0.2 ns, raising the temperature by 50 K each, until reaching 300 K, all in the presence of the constraints reported in Supplementary Table 2.
4. Use of 1.2-ns MD simulations at room conditions (300 K and 1 atm), in which the harmonic constraints were progressively removed.
5. Use of 6.3-ns unconstrained MD simulations.

Additionally, shorter MD simulations of P/CAF mutants Tyr760Asp and Tyr761Asp were performed to check the relevance of these positions for the protein–protein interaction. Both mutants were constructed over the last snapshot of the constrained dynamics (time = 1.2 ns) by replacing the corresponding residues. Since Tyr's are bigger residues than Asp, their mutation did not generated steric clashes. To avoid spurious distortions due to the abrupt perturbation, we applied again the same set of constraints used during the stabilization phase and decreased them over 0.3 ns. Finally, 4 ns of unconstrained MD simulation were run for both systems.

MD simulations on AcK50 Tat peptide-P/CAF bromodomain

As a control case we performed a simulation of the AcK50 Tat peptide-P/CAF using the conformer 13 of the NMR family. The peptide–protein complex was immersed in a rectangular box containing ~8000 water molecules and 10 neutralizing Cl^- counterions. This peptide–protein complex underwent first energy minimization and then thermalization with an identical setup and parametrization used for the protein–protein complex, but no constraints were imposed. An MD simulation of 2.5 ns was performed and compared with the structural determinants obtained by NMR.

Simulations using different starting conformers

To further assess the reliability of our theoretical model, we sought to perform MD simulations using the general-

ized Born (GB) implicit solvation method.[34] We therefore performed MD simulations arbitrarily choosing as starting structures the NMR conformers 1, 9, 13, and 25. As in the case of explicit solvent simulation, 1.2 ns of constrained MD followed by 4 ns of fully unconstrained simulations were performed using the SANDER module of AMBER 8.0.

The following properties were calculated:

1. RMSDs from the initial position, instantaneous distances, and H-bonds patterns were calculated as in Pantano et al.[27]
2. Solvent-accessible surfaces in the ZA loop were calculated using a proof radius of 1.4 Å[35] from Glu750 to Asp769.
3. Hydrophobic contacts were considered to exist between CH_n carbons within a cutoff distance of 4.5 Å.
4. Accessible solvent areas (ASAs) at the protein–protein interface were calculated using the Protein–Protein Interactions server (http://www.biochem.ucl.ac.uk/bsm/PP/server/index.html). An average ASA over the MD snapshots at 4 ns, 5 ns, 6 ns, and 7 ns was calculated.
5. The free energy of binding was calculated as $G_{bind} = G_{el} + G_{np}$, where G_{el} and G_{np} are the electrostatic and nonpolar energy contributions, respectively.[36] The electrostatic contribution is obtained as the sum of a Coulomb term (accounting for the work needed to assemble the protein taking the charges from the infinite) plus a reaction field term (accounting for the work required to change the dielectric permittivity from the external—water–to the internal—protein—media). We obtained electrostatic contributions by numerically solving the Poisson–Boltzmann equation with DELPHI,[37] using the AMBER94 force field parameterization[32] for partial charges and van der Waals radius. A box filling of 80% is adopted with a scale of 2 grid points per Å with Coulombic boundary conditions. Nonpolar solvation contribution to binding energy was estimated using the expression $G_{np} = \gamma ASA$, where $\gamma = 0.025$ kcal/(mol Å^2).

These expressions are only approximate and have been used here only as a rough estimation of the binding energies. The free energy gain upon complex formation was estimated as $\Delta G_{bind} = G_{complex} - G_A - G_B$, where the suffixes A and B stand for the free forms of P/CAF and the Tat peptide or the full length Tat protein. Since important structural changes take place upon binding, we used (1) for P/CAF, the NMR-derived free form[23]; since the residues determined in the structure of free P/CAF and in complex with the peptide differ in the number or residues, a polypeptide chain from Asp726 to Ala827 spanning the whole helix bundle and loops was considered; (2) for the peptide, the same structure obtained in complex with P/CAF, as it is very likely unstructured and extended in solution; (3) for Tat, the conformer of AcK50 Tat from a MD simulation used as starting structure of the complex (see above).

Plasmids and Cells

The expression plasmid pcDNA3-Tat-BFP was previously characterized.[38] Plasmid pGEX-P/CAF, kindly provided by Monsef Benkirane (IGH, CNRS; Montpellier, France), was used as a template for the mutagenesis. pGEX-P/CAFY760D and pGEX-P/CAFY761D were obtained by polymerase chain reaction (PCR) mutagenesis with common external primers P/CAFFW 5′-CATCCTGAACTTCCTCACATA-3′ and P/CAFRV 5′-CCGCTCGAGTCACTTGTCAATTAATCC-3′, and specific internal mutagenesis primers, either P/CAFY760DFW 5′-GCTCCAGGAGATTATGAAGTT-3′ plus complementary sequence, or P/CAFY761DFW 5′-GCTCCAGGATATGATGAAGTT-3′ plus complementary sequence. Modified PCR products were cloned as NdeI/XhoI fragments back in pGEX-P/CAF and sequenced. Enhanced green fluorescent protein (EGFP)-tagged derivatives were obtained by subcloning the EcoRI/XhoI fragment from the pGEX4-T2 constructs into the EcoRI/SalI sites of pEGFP-C2 (Clontech; Palo Alto, CA). The cell lines used in this study were cultured in Dulbecco's modified Eagle's medium (DMEM) supplemented with 10% fetal bovine serum.

HAT Assay

HAT assay was performed as previously reported with minor modifications.[9] glutathione transferase (GST) fusion proteins were incubated with ^{14}C-Acetyl-CoA in HAT buffer [50 m*M* Tris, pH 7.5, 5% glycerol, 0.1 m*M* ethylene diaminetetraacetic acid (EDTA), 50 m*M* KCl, and 2 m*M* sodium butyrate] containing 1 μg of calf thymus histones in a final volume of 20 μL for 45 min at 30°C. Autoacetylated P/CAF and acetylated histones were visualized by phosphoimaging after separation by 4–20% gradient sodium dodecyl sulfate–polyacrylamide gel electrophoresis (SDS-PAGE).

Fluorescence Resonance Energy Transfer (FRET)

HeLa cells were transiently transfected using Effectene (Qiagen) in four-chamber glass slides. Cells were fixed in 4% paraformaldehyde after 48 h and mounted directly in 70% glycerol for FRET analysis. FRET measurements were carried out as previously described[38,39] by an epifluorescence Axioskop 2 Zeiss microscope mounting a 103 W HBO lamp, a 100× 1.3 N.A. oil-immersion Plan-Neofluar objective, and Nomarski optics. FRET analysis was performed in two steps. First, EGFP emission was collected by integrating the fluorescence signal around 520 nm (bandwidth 40 nm) under EGFP excitation at 480 nm (wavelength selection was obtained by 40 nm band-pass filters, excitation power was 5 W/cm^2). Second, EGFP emission in the same frequency range was measured after excitation at 350 nm (power density 2 W/cm^2 and bandwidth 60 nm). The background was determined for each frame by measuring the signal outside the cell under study and subtracting its value from the relevant fluorescent signal. Following this procedure, the ratio between the two measured EGFP emissions (data taken following excitation at 350 nm divided by those at 480 nm) yielded the FRET signal. Fluorescence was collected by a PentaMax 512-EFT intensified charge-coupled device (CCD) camera with detection times in the order of 0.1 s (in particular, for data taken under excitation at 350 nm, they were five

times longer than for those relative to 480-nm excitation). Data acquisition and analysis were performed with the Metamorph software. When evaluating FRET ratios, emission intensities were scaled to take into account the different detection times.

Transcription Assays

HeLa cells were transfected in triplicate using Effectene (Qiagen) in 24 well plates with the reporter construct LTR-luciferase,[40] the expression vector for HIV-1 Tat pcDNA3Tat86,[38] and increasing amounts of the various P/CAF constructs. The dual-luciferase assay from Promega was used to determine the activity of the promoter normalized with the Renilla reference.

RESULTS

Tat:P/CAF Complex Structure From MD Simulations

Because Tat binds in vivo to many cellular partners (e.g., P-TEFb, TAR, etc.) other than P/CAF, we focused here only on the contacts at the protein–protein interface of Tat:P/CAF BD complex.

The structural model of P/CAF BD:AcK50 Tat was based on the family of NMR structures of the P/CAF BD in complex with the acetylated SYGRAcK_{50}KRRQC peptide[21] and on a structure of AcK50 Tat in aqueous solution, as obtained previously from a 3-ns MD simulation.[24] The solution structure of AcK50 Tat was fitted (see Methods section) onto the AcK50 binding site of the BD. Since normal energy minimization protocols lead to complex conformations corresponding to local energy minima near to the starting configuration, we decided to perform MD simulations in water solution at room temperature and pressure, since it is expected that temperature effects may allow the entire complex to explore the energy landscape obtaining a better relaxation.

General features

After a stabilization period of about 3 ns of MD simulation, the RMSD of each of the proteins turned out to oscillate around a relatively high value (3.8 Å) with respect to the initial structure (Supplementary Fig. 1a). This points to important conformational changes due to a mutually induced fit. The distance between the centers of mass of the two proteins rose from 32 Å to 34 Å after the constraints were released (see Methods section), then oscillated around this value (Supplementary Fig. 1a). This clearly indicates no tendency of the complex to dissociate. The final minimized structure of the adduct exhibited 90% of the residues in the most favored regions of the Ramachandran map and no residues in disallowed regions.

The left-handed, four-helix bundle motif of P/CAF was fully maintained in the complex structure. Only small changes were observed in the short BC loop [Fig. 1(b)], probably due to the rigidity provided by the two consecutive prolines at positions 804 and 805. Instead, the flexible ZA loop underwent important changes upon Tat binding [Fig. 1(b)]. Calculation of the RMSD on the different structural motifs of P/CAF indicates that only within the AZ loop reaches 3.7 Å, while the remaining part of the protein features only 1.4 Å, indicating that conformational changes associated to the complex formation are mainly limited to the protein–protein interface. The AZ loop exhibited a compact conformation in the free state[23] and an extended conformation in the peptide–protein complex,[21] which was even more extended in the protein–protein complex. Indeed, the solvent-accessible surface[35] of the ZA loop changed from 1468 $Å^2$ in free state to 1584 $Å^2$ in the peptide-bound state and to 1661 $Å^2$ in the full length Tat-bound state (Supplementary Fig. 2). An average number of nine water molecules partly solvated the polar moiety of AcK50, the conformation of which is alike to that of the NMR structure.[21] The same number of water molecules was found inside the binding pocket of the histone acetyltransferase GCN5P BD bound to acetylated peptide of the Histone H4.[41]

Analysis of binding energy

Comparison of ASA between the protein–peptide and protein–protein complexes gives, as expected, a larger interface area for the latter (Supplementary Table 3), indicating a gain of about 4 kcal/mol due to nonpolar interactions. Calculation of the electrostatic binding energy for the P/CAF-peptide gives a modest gain upon complexation of nearly 2 kcal/mol, while the P/CAF-AcK50Tat obtained by MD gives about 44 kcal/mol. Taken together, it provide a free energy difference between both complexes ($\Delta\Delta G_{\mathrm{Bind}}$) of roughly 46 kcal/mol.

AcK50 Tat:P/CAF contacts

[For clarity, the P/CAF residues are written in *italics* to distinguish them from the Tat residues.] Three domains of Tat were found to interact with the BD binding site, namely, the N-terminal domain, the hydrophobic core region, and the basic domain [Fig. 1(c–f)]. In the N-terminal domain, Met1 formed hydrophobic interactions with *Pro804*, *Pro805*, and *Ser807* within the BC loop of the P/CAF BD [Table I, Fig. 1(c)]. Strong electrostatic repulsions between Asp2/5 and *Glu801/806/808* might prevent the formation of other contacts between the two regions.

The core domain of Tat formed several interactions that did not emerge in the previously determined NMR structure [Table I, Fig. 1(c)]. In fact, Ile39, Gly42, Gly44, Ile45, and Gly48 interacted with hydrophobic moieties within the P/CAF ZA loop [Table I, Fig. 1(e)], and, in particular, with *Tyr761*, which was instead completely solvent-exposed in the NMR structure and in the initial MD model (see animation at ftp://ftp.icgeb.org/pub/tmp/tatpcaf.mov). Thus, the structure evolves toward a more compact packing of the hydrophobic residues within the protein–protein interface. This generates the formation of hydrophobic clusters [Fig. 2(a)] composed by the residues reported in Table I.

The Tat residue Tyr47 did not interact with *Val763*, as reported in the NMR peptide-bound structure, while it formed hydrophobic contacts with Val4, Pro10, and Leu43 in Tat itself [Fig. 1(f)].

The Tat basic domain formed contacts similar to those of the NMR structure (Table I). In particular, both the

TABLE I. Hydrophobic Contacts Between CH_n Carbons Belonging to Residues in the Protein–Protein Interface

Full-length Tat interface residues	P/CAF BD interface residues (MD)	% occupancy	Tat peptide interface residues	P/CAF BD interface residues (NMR)
Met1	Pro804	100	Tyr47	Val763
	Pro805	21		Gly759
	Ser807	60		Tyr802
Gly42	Tyr761	100	Gly48	Gly759
Ile39	Tyr761	80		Tyr760
Gly44	Tyr761	100		Val763
Ile45	Pro758	72		Tyr802
	Tyr761	46	Arg49	Ala756
Gly48	Val763	100		Pro768
	Ile764	100		Tyr802
	Tyr802	100	AcK50	Tyr760
Arg49	Tyr802	30		Tyr802
AcLys50	Phe748	100		Cys799
	Val752	100		Tyr809
	Tyr760	30		Asp745
	Tyr761	30	Lys51	Pro748
	Val763	100	Arg53	Glu756
	Ile764	100	Gln54	Glu756
	Asp769	100		
	Val795	21		
	Tyr802	100		
Lys51	Glu750	48		
	Ala757	85		
	Tyr809	39		

Left: Calculated over the last 4 ns of MD simulations. Only occupancies higher than 20% are reported. Right: Calculated over the peptide-P/CAF BD structure (NMR).

AcK50/*Asp789* interaction and the extended conformation of the AcK50 side-chain present in the NMR structure were fully maintained in the MD simulation (Table II). Interestingly, both features were similar to those found in the three BD/AcK complex structures so far available.[21,41,42] Gln54 did not form H-bonds with the *Glu756* backbone as in the NMR structure. Instead, it was fully solvated, while its side-chain methylene carbons formed hydrophobic interactions with Met1. In addition, Lys51, which interacts with *Glu750*, was fully solvated in the NMR structure.

Considering all of the above, we conclude that most of the contacts present in the NMR structure of the acetylated Tat peptide with the P/CAF BD were also conserved in our MD simulation, although the full length Tat protein imposed structural constraints that determined important differences, as evidenced by the percentual contributions of the individual residues to the protein–protein interface [Fig. 2(b]. Looking to the Tat side, we observe that the main contribution in both cases come from AcK50, while interactions of Ser46, Tyr47, Gln54, and Arg55 present in the peptide bound structure were lost in the full-length case. In the latter, the distribution of the contacts is broader as new contacts arose from different parts of the protein (e.g., Met1, Ile39, Lys41, Gly42, Gly44, and Arg53). Form the P/CAF side, we observe that the most relevant contributions to the interface (e.g., those from *Tyr760*, *Glu762*, *Val763*, *Tyr802*, and *Tyr809*) were conserved, while new, important contacts were contributed by *Glu750*, *Tyr761*, *Pro804*, and *Glu808*.

Despite the high density of basic–acidic residues in the Tat basic region and in the P/CAF BD mouth (Supplementary Fig. 3), only a few H-bonds or salt bridge interactions were established (Table II, Fig. 1). This fact underlines the highly hydrophobic nature of this protein–protein interaction[43] and the relevance of the long hydrophobic chain at position 50 in Tat.[24]

MD simulations on P/CAF mutants

In our aim to further investigate the complex stabilization by hydrophobic residues at the protein–protein interface, we sought to perform MD simulations mutating key residues that formed extended contacts at the protein–protein interface. Our calculations suggest that the change from a hydrophobic to a hydrophilic amino acid within the AZ loop of P/CAF should affect the interactions with the hydrophobic core of Tat. Given the high degree of flexibility and promiscuity of Tat, we focused on changes in the P/CAF ZA loop that are not likely to affect the global conformation of the BD [Fig. 1(b)]. Within this loop, *Tyr761* forms the most extensive hydrophobic contacts, and is either highly conserved or conservatively mutated to phenylalanine in several BDs.[44] An additional critical residue is the neighboring amino acid, *Tyr760*, which is turned toward the hydrophobic cleft in the P/CAF BD and

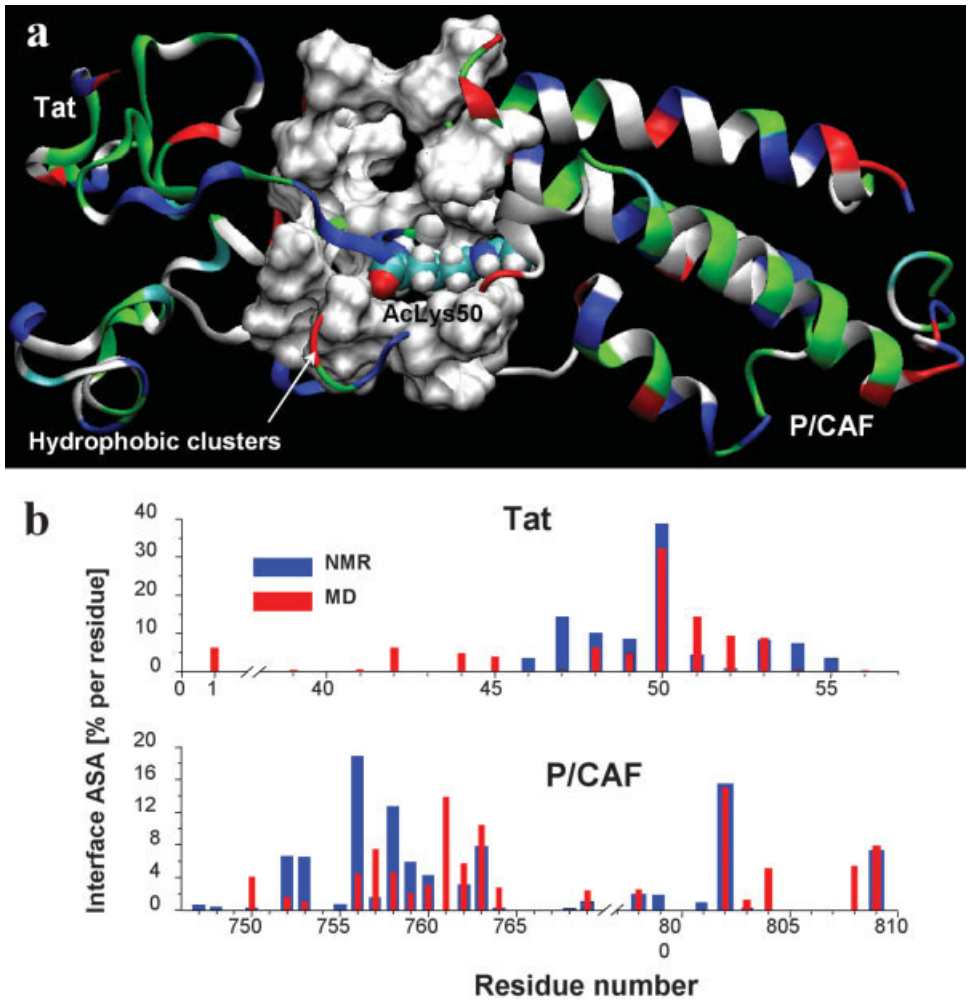

Fig. 2. Characterization of the protein–protein interface. (**a**) Cartoon representation of the AcK50 Tat:P/CAF BD. The solvent-accessible surface of the residues forming hydrophobic clusters are represented in white. The cluster shown is formed in Tat by Met1, Pro3, Val4, Pro6, Ile39, Gly42, Leu43, Gly44, Ile45, and Tyr47, and in P/CAF BD by Pro751, Val752, Ala757, Pro758, Gly759, Tyr760, Tyr761, Val763, Ile764, Tyr802, Pro804, Pro805, and Tyr809. AcK50 is presented as van der Waals spheres colored by atom. (**b**) Comparison between the residue contributions to the interface ASA expressed in percent of the total interface ASA for the NMR[21] and MD structures presented in Figure 1. [Color figure can be viewed in the online issue, which is available at www.interscience.wiley.com.]

TABLE II. Selected Interprotein H-Bond Interactions

Donor–Acceptor	Avg. distance (Å)	% occupancy
Salt bridges		
Lys51–Glu750	3.0 (0,4)	95
Arg53–Glu808	3.1 (0,4)	35
H-bonds		
Arg52 (Nη)–Glu756 (O)	3.1 (0,3)	64
Glu762 (N)–Gly42 (O)	3.4 (0,3)	51
Asn798 (Nδ)–AcK50 (O acetyl)	3.3 (0,4)	25
Tyr802 (OH)–AcK50 (O acetyl)	3.2 (0,4)	25

Standard deviations are reported in parentheses. Only occupancies higher than 20% are reported. The only conserved interaction corresponding to AcK50-Asn798 is underlined.

forms contacts with the AcK50 of Tat.[21,23] Although the timescale available to state-of-the-art simulations is not long enough to show a dissociation of the complex, we found, in agreement with our previous conclusions, that both P/CAF mutants resulted in a destabilization of the complex. The simulation of the mutant *Y760D* resulted in notably higher RMSDs (Supplementary Fig. 1b), still increasing after 5.5 ns of simulations. The whole complex and P/CAF reached 5.3 Å, while Tat arrived to 6.6 Å. The distance between the centers of mass of both proteins in this mutant complex remained at values near 33.5 Å comparable to that of the wild-type. The *Y761D* mutant complex suffered larger distortions, with all RMSD curves showing a continuous increase at 5.5 ns of simulation, reaching values of 7.5 Å, 5.3 Å, and 5.7 Å for the whole complex, Tat, and P/CAF, respectively (Supplementary Fig. 1c). Also the distance between the centers of mass of this mutant complex showed an enlargement, suggesting a marked tendency to dissociation.

Reliability of the MD Model

To ascertain that the outcome of the full protein–protein simulation was not due to artifacts of the theoretical treatment, particularly regarding the specific interactions of the nonstandard residue AcK50, we performed a 2.5-ns-long MD simulation of the complex between the acetylated Tat peptide (SYGRAcK50 KRRQC) and P/CAF's BD as found in the PDB database (model 13). No remarkable changes were observed in the conformation of both molecules or in their reciprocal orientation. The RMSD on the adduct backbone stabilizes after 0.6 ns, oscillating around 1.7 Å (data not shown), which is well compatible with the structural dispersion found among the NMR family.

To further assess the reliability of our theoretical model, we performed a number of additional MD simulations. First, we performed a 2.5-ns-long MD simulation of the complex between the acetylated Tat peptide (SYGRAcK50KRRQC) and P/CAF's BD as found in the PDB database (model 13). The peptide–protein complex underwent first energy minimization and then thermalization identical to the case of the protein–protein complex, but no constraints were imposed. No remarkable changes were observed in the conformation of both molecules or in their reciprocal orientation. The RMSD on the adduct backbone stabilizes after 0.6 ns, oscillating around 1.7 Å (data not shown), which is well compatible with the structural dispersion found among the NMR family. Second, we performed MD simulations on the entire complex using the GB implicit solvation method.[34] This method provides a faster, although less accurate, description than that obtained using explicit water molecules. We therefore performed MD simulations within the framework of GB using an identical setup to the previous MD simulation based on randomly chosen NMR structures (namely, NMR conformers 1, 9, 13, and 25). Although the final structures obtained display different conformations, with an average RMSD of 4 Å (data not shown), they all present extended hydrophobic interactions within the protein–protein interface. In particular *Tyr760* and *Tyr761* in P/CAF are always involved in the formation of hydrophobic clusters similar to those described above.

Experimental Validation of the MD Model

To experimentally ascertain the relevance of *Tyr760* and *Tyr761* in maintaining the interaction between AcK50Tat and P/CAF, we selectively mutated them to aspartate, since our calculations suggested that the change from a hydrophobic to a hydrophilic amino acid should affect the interaction of the protein with the hydrophobic core of Tat.

Functional characterization of the P/CAF mutants

Wild-type P/CAF and the P/CAF mutants *Y760D* and *Y761D* were obtained as recombinant proteins fused to GST, and their enzymatic activity was tested. As shown in Figure 3(a), both the wild-type protein and the two mutants, but not unfused GST, were able to acetylate histones, and, in particular, H3. In addition, all three proteins displayed autoacetylation activity [Fig. 3(b)]. These observations clearly indicate that the *Y760D* and *Y761D* mutations do not impair the enzymatic activity of P/CAF. Next, expression vectors were obtained for two mutants, as well as for wild-type P/CAF, in which the proteins had EGFP fused at their N-terminus. Wild-type EGFP-P/CAF and the two mutants were cotransfected in HeLa cells together with an expression vector for Tat and an LTR-luciferase reporter. In the presence of suboptimal concentrations of Tat, the HIV-1 promoter was clearly coactivated by wild-type P/CAF but not by either of the two mutants [Fig. 3(c)].

Visualization of in vivo interaction between P/CAF and Tat by FRET

The lack of functional coactivation of Tat-mediated transcription by the two P/CAF mutants is consistent with the possibility that the two mutations impair binding of the two proteins, either by disrupting the hydrophobic pocket that homes AcK50 (*Y760D*) or by hindering contacts between the BD and the Tat core (*Y761D*). Therefore, we set out to directly visualize the binding between Tat and P/CAF inside the cells by FRET using the two proteins tagged with the BFP:EGFP fluorescent protein pair. FRET consists of radiationless energy transfer driven by dipole–dipole interaction between one fluorophore (the donor) in the excited state and another fluorophore (the acceptor) when in close proximity. As a result of FRET, donor excitation is followed by energy transfer and acceptor fluorescence.[45–47] Simple colocalization of two proteins is not sufficient to yield energy transfer, which requires the proximity of the two fluorophores at distances that, in most cases, are on the order of few nanometers.[48–50] Thus, the presence of FRET between two proteins most likely indicates direct protein–protein interaction. Recently, we have exploited the EGFP:BFP fluorescent protein pair to monitor the intracellular interaction of human cyclin T1 with HIV-1 Tat[38] and human PML by FRET.[39]

FRET experiments between P/CAF and Tat were performed by transfection of HeLa cells with plasmids expressing EGFP fused at the C-terminus of wild-type P/CAF or the P/CAF mutants together with Tat-BFP, followed by the analysis of fluorescence at 520 nm (the peak wavelength of EGFP emission). The presence of FRET indicates actual protein–protein interaction at distances in the range of the FRET length scale, the Förster radius (R_0), defined as the distance at which FRET efficiency (E_T) is 50%. E_T is defined as the ratio between the sixth power of R_0 and the sum of the sixth power of R_0 and the sixth power of R, with R being the actual distance between the donor and the acceptor fluorophores. E_T dramatically decreases when R increases by a fraction of the nanometer (nm) around R_0, which, in the case of the BFP:EGFP fluorescent protein pair, is ≈ 4 nm.[51] Thus, the presence of FRET between two proteins tagged with this fluorescent protein pair implies the existence of direct protein–protein interaction.[48–50] Representative results of these experiments are shown in Figure 4(a). The panels in row b show the intracellular distribution of fluorescence at 520 nm under excitation at 480 nm, characteristic of EGFP. FRET analysis was performed by comparing acceptor EGFP emission at 520 nm, following donor BFP excitation at 350

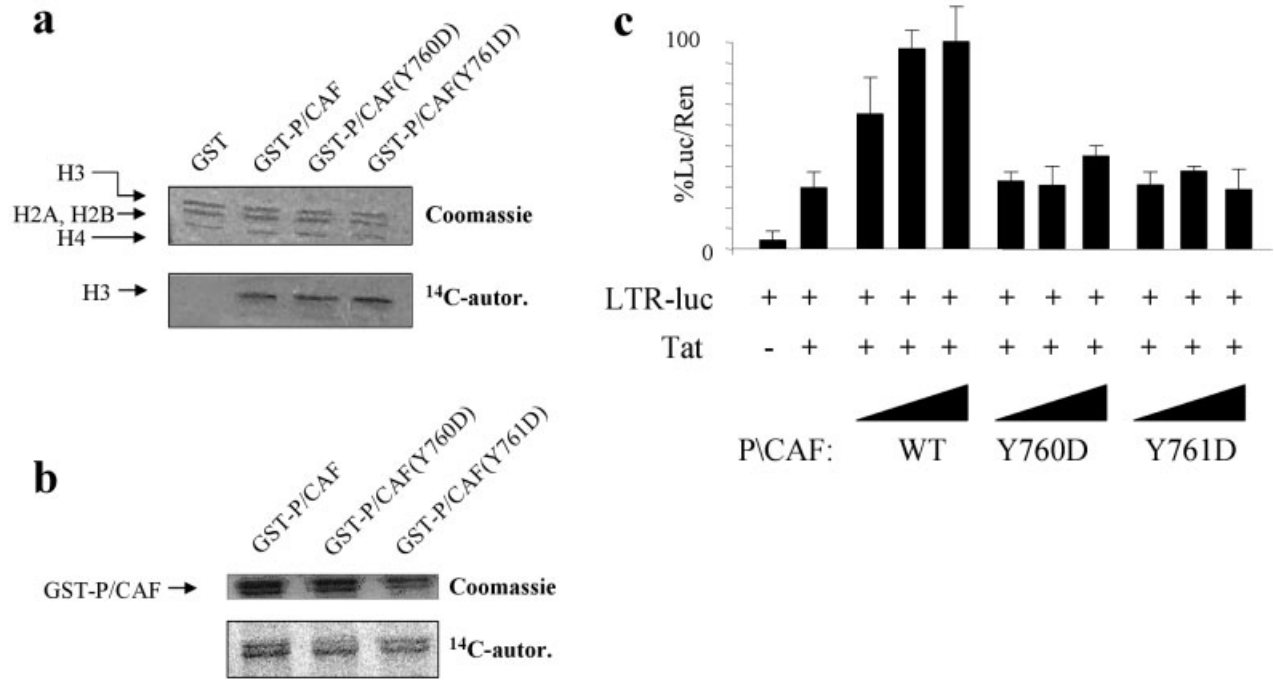

Fig. 3. Functional activity of P/CAF and mutants. (**a**) Histone acetylation. Recombinant proteins were incubated with labeled acetyl-CoA and calf thymus histones in HAT buffer. Both *Y760D* and *Y761D* are capable of acetylating histones (and, in particular, H3) as the wild-type P/CAF protein. (**b**) P/CAF autoacetylation. As in (a) but measuring autoacetylation of P/CAF and its mutant derivatives. (**c**) Stimulation of Tat activity by wild-type, EGFP-tagged, P/CAF and by the *Y760D* and *Y761D* P/CAF mutants. HeLa cells were cotransfected with the LTR-luciferase reporter (100 ng) and a limiting amount of pcDNA3-Tat86 (5 ng), together with increasing amounts of the EGFP-tagged constructs (2.5 ng, 5.0 ng, and 7.5 ng), as indicated. Data are presented as a percentage after normalization with cotransfected pCMV-Renilla.

nm [Fig. 4(a), panels in row c], with that following excitation at 480 nm of the same cells [Fig. 4(a), panels in row b]. In these conditions, the samples expressing both EGFP-P/CAF wild-type and Tat-BFP scored positive for FRET, indicating direct interaction between the two proteins. In contrast, no FRET was observed between Tat and the nucleolar protein fibrillarin, despite the localization of the latter protein in the same compartments as Tat.[52] We can therefore conclude that P/CAF and Tat directly interact within the nucleus of cotransfected cells. Next we extended this experiment to the P/CAF mutants. Both mutations *Y760D* and *Y761D* completely abolished the FRET signal [Fig. 4(a)], indicating that the two proteins were no longer at a distance favorable for FRET. The detailed, quantitative analysis of at least 10 expressing cells for each of the analyzed protein pairs is presented in Figure 4(b), showing the percentile distribution of FRET values.

DISCUSSION

BDs are highly conserved recognition motifs for proteins acetylated at specific lysine residues.[44] Ligand selectivity depends on variations in the BD ZA loop, which has low sequence conservation among the different BDs, and on the boundaries of the acetylated lysine. Beyond acetylated histones, HIV-1 Tat acetylated at Lys50 is the best characterized ligand for the P/CAF BD.[19–21,53]

Based on the NMR structure of an acetylated Tat peptide in complex with the P/CAF BD, we obtained by MD simulations a model of the interaction between acetylated full-length Tat with P/CAF BD. We must note that due to the intrinsic limitations of the theoretical treatment added to the large sequence and structure variability displayed by the Tat protein,[54] the complex obtained here may not be referred as an atomic-detail model. Furthermore, it cannot be ruled out that the concomitant binding to Tat by other binding partners, such as cyclin T1, for example, may produce further conformational modifications in regions other than the protein–protein surface. Those interactions cannot be modeled at the present stage because of the lack of structural information. Nevertheless, our theoretical approach allowed us to individuate some key residues for the complex formation. The reliability of the modeling limited to the single amino acid level within the AcK50 Tat:P/CAF BD interface, which is the focus of this study, has been supported by a number of MD simulations on the Tat:P/CAF wild-type complex, on point mutants *Y760D* and *Y761D* within the AZ loop of P/CAF, on different starting conformers using the GB model implicit solvation, as well as by mutagenesis experiments performed here. The main outcome of our work is that binding between the two proteins involve the Tat core and the BD ZA loop hydrophobic regions. On the Tat side, of particular note is the observation that residue Tyr47 does not appear to interact with *Val763* of P/CAF, as reported in the NMR peptide-bound structure. We found rather that this residue forms hydrophobic contacts with the Tat N-terminus and Leu43. Since the mutation of this tyrosine to alanine impairs Tat transactivation,[19] we suggest that this amino

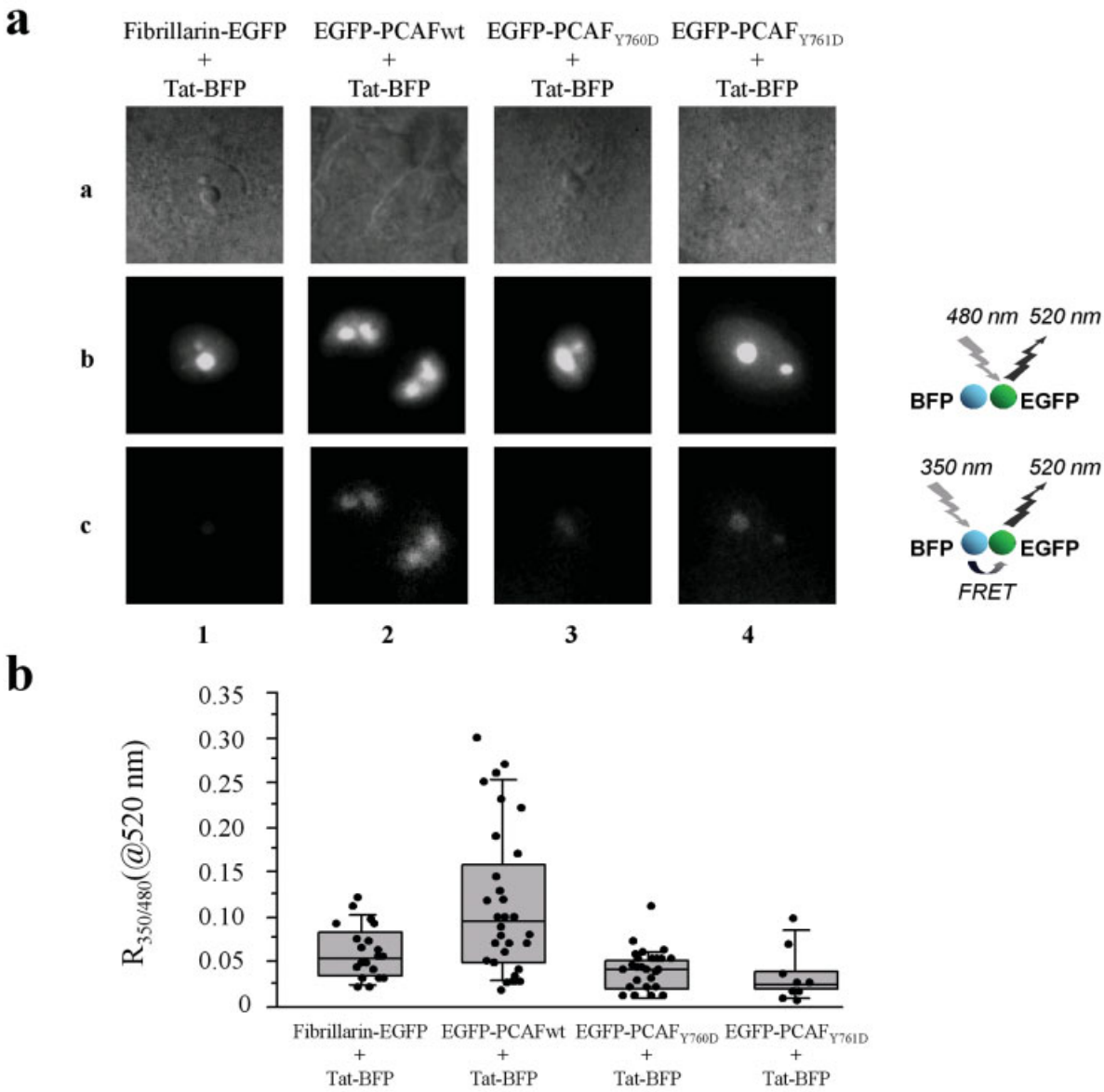

Fig. 4. FRET analysis of protein–protein interactions in vivo. (**a**) Visualization of FRET. The plasmid constructs indicated on top of each column were transfected in HeLa cells. Transfected cells were visualized by transmitted light in Nomarski configuration (panels in row a), by excitation at 480 nm and collection at 520 nm, showing EGFP fluorescence after direct EGFP excitation (panels in row b), and by excitation at 350 nm and collection at 520 nm, showing EGFP fluorescence after BFP excitation, indicating FRET (panels in row c). (**b**) Quantification of FRET. Fluorescent emission at 520 nm from individual cells transfected with the indicated constructs was recorded after excitation at 350 nm or 480 nm, and integrated intensities over the whole cell were evaluated. Plotted values (indicated by dots) represent the ratio between these two measurements: Higher values indicate more efficient resonant energy transfer between BFP and EGFP. At least 10 consecutively analyzed cells were considered for each transfection; both their individual fluorescence ratio and their percentile box-plot distribution are shown. Horizontal lines of the percentile box plot distribution of FRET values, from top to bottom, mark the 10th, 25th, 50th, 75th, and 90th percentiles, respectively. [Color figure can be viewed in the online issue, which is available at www.interscience.wiley.com.]

acid may be important to either preserve the protein structure[24] or to allow binding with other cellular targets, such as TAR,[55] rather than being involved in the interaction with P/CAF.

In our MD model, the Tat AcK50 hydration properties, as well as the AcK50 mode of binding, turned out to be almost identical to those found in the structurally similar GCN5 BD binding an acetylated peptide derived from the H4 histone, for which the X-ray structure had been determined.[41] This suggests that acetylated lysines bind this class of proteins in a rather similar manner. However, when the P/CAF BD MD model is compared to the NMR structures of the free P/CAF BD[23] and the P/CAF BD bound to the acetylated Tat peptide,[21] an increased degree of exposition of the BD ZA loop was observed, which determines a decrease in its compactness (Supplementary Fig. 2). This may indicate that in the presence of the full length Tat protein, the ZA loop does not tightly fold to form

a hydrophobic environment for the acetylated lysine, as previously believed, but rather offers a highly adaptable platform for more extended ligand recognition. This observation might provide a structural basis to explain the specific BD selectivity.[56] Our model suggests that the free energy of complexation is lower than that of the complex with the acetylated peptide, because of the increase of the hydrophobic effect. Experimentally, we also expect that the contribution of the full-length Tat protein to the binding shifts the association constant from the micromolar range estimated for the peptide to nanomolar range in the case of the full Tat, as the viral protein must compete for the binding site with other cellular proteins.

In this context, the positions of two contiguous tyrosine residues in the P/CAF BD are particularly important: Whereas Tyr760 is part of the cleft that accommodates the acetylated lysine, *Tyr761* makes several hydrophobic contacts with residues in the core domain of Tat. The mutation of either of these two tyrosines not only impairs P/CAF coactivation of Tat-mediated transcription, but it more specifically blocks Tat binding to P/CAF, as concluded from the absence of FRET between Tat and the two mutants. With the obvious limitation that the FRET experiments were performed in cells overexpressing the two tagged proteins, the presence of FRET between Tat and P/CAF shown here is the first demonstration that the two proteins physically interact within the cell nucleus. From the FRET results, we cannot rule out that the interaction between the two proteins in vivo might also occur in the absence of Tat acetylation, as has been shown in vitro.[10] However, the observation that the two P/CAF BD mutants at *Tyr760* and *Tyr761* are both impaired in transactivation and fail to give FRET is in agreement with the structural prediction that these two amino acids are essential to maintain the contacts between Tat acetylated at Lys50 and the BD.

REFERENCES

1. Dingwall C, Ernberg I, Gait MJ, Green SM, Heaphy S, Karn J, Lowe AD, Singh M, Skinner MA, Valerio R. Human immunodeficiency virus 1 Tat protein binds trans-activation-responsive region (TAR) RNA in vitro. Proc Natl Acad Sci USA 1989;86:6925–6929.
2. Berkhout B, Silverman RH, Jeang KT. Tat trans-activates the human immunodeficiency virus through a nascent RNA target. Cell 1989;59:273–282.
3. Marcello A, Zoppe M, Giacca M. Multiple modes of transcriptional regulation by the HIV-1 Tat transactivator. IUBMB Life 2001;51:175–181.
4. Karn J. Tackling Tat. J Mol Biol 1999;293:235–254.
5. Wei P, Garber ME, Fang S-M, Fisher WH, Jones KA. A novel CDK9-associated C-type cyclin interacts directly with HIV-1 Tat and mediates its high-affinity, loop-specific binding to TAR RNA. Cell 1998;92:451–462.
6. Price DH. P-TEFb, a cyclin-dependent kinase controlling elongation by RNA polymerase II. Mol Cell Biol 2000;20:2629–2634.
7. Verdin E. DNase I-hypersensitive sites are associated with both long terminal repeats and with the intragenic enhancer of integrated human immunodeficiency virus type 1. J Virol 1991;65:6790–6799.
8. Verdin E, Paras P Jr, Van Lint C. Chromatin disruption in the promoter of human immunodeficiency virus type 1 during transcriptional activation. EMBO J 1993;12:3249–3259.
9. Marzio G, Tyagi M, Gutierrez MI, Giacca M. HIV-1 Tat transactivator recruits p300 and CREB-binding protein histone acetyltransferases to the viral promoter. Proc Natl Acad Sci USA 1998;95:13519–13524.
10. Benkirane M, Chun RF, Xiao H, Ogryzko VV, Howard BH, Nakatani Y, Jeang KT. Activation of integrated provirus requires histone acetyltransferase: p300 and P/CAF are coactivators for HIV-1 Tat. J Biol Chem 1998;273:24898–24905.
11. Col E, Caron C, Seigneurin-Berny D, Gracia J, Favier A, Khochbin S. The histone acetyltransferase, hGCN5, interacts with and acetylates the HIV transactivator, Tat. J Biol Chem 2001;276:28179–28184.
12. Kamine J, Elangovan B, Subramanian T, Coleman D, Chinnadurai G. Identification of a cellular protein that specifically interacts with the essential cysteine region of the HIV-1 Tat transactivator. Virology 1996;216:357–366.
13. Weissman JD, Brown JA, Howcroft TK, Hwang J, Chawla A, Roche PA, Schiltz L, Nakatani Y, Singer DS. HIV-1Tat binds TAFII250 and represses TAFII250-dependent transcription of major histocompatibility class I genes. Proc Natl Acad Sci USA 1998;95:11601–11606.
14. Lusic M, Marcello A, Cereseto A, Giacca M. Regulation of HIV-1 gene expression by histone acetylation and factor recruitment at the LTR promoter. EMBO J 2003;22:6550–6561.
15. Deng L, de la Fuente C, Fu P, Wang L, Donnelly R, Wade JD, Lambert P, Li H, Lee CG, Kashanchi F. Acetylation of HIV-1 Tat by CBP/p300 increases transcription of integrated HIV-1 genome and enhances binding to core histones. Virology 2000;277:278–295.
16. Kiernan RE, Vanhulle C, Schiltz L, Adam E, Xiao H, Maudoux F, Calomme C, Burny A, Nakatani Y, Jeang KT, Benkirane M, Van Lint C. HIV-1 Tat transcriptional activity is regulated by acetylation. EMBO J 1999;18:6106–6118.
17. Ott M, Schnolzer M, Garnica J, Fischle W, Emiliani S, Rackwitz HR, Verdin E. Acetylation of the HIV-1 Tat protein by p300 is important for its transcriptional activity. Curr Biol 1999;9:1489–1492.
18. Bres V, Kiernan R, Emiliani S, Benkirane M. Tat acetyl-acceptor lysines are important for human immunodeficiency virus type-1 replication. J Biol Chem 2002;277:22215–22221.
19. Dorr A, Kiermer V, Pedal A, Rackwitz HR, Henklein P, Schubert U, Zhou MM, Verdin E, Ott M. Transcriptional synergy between Tat and PCAF is dependent on the binding of acetylated Tat to the PCAF bromodomain. EMBO J 2002;21:2715–2723.
20. Kaehlcke K, Dorr A, Hetzer-Egger C, Kiermer V, Henklein P, Schnoelzer M, Loret E, Cole PA, Verdin E, Ott M. Acetylation of Tat defines a cyclinT1-independent step in HIV transactivation. Mol Cell 2003;12:167–176.
21. Mujtaba S, He Y, Zeng L, Farooq A, Carlson JE, Ott M, Verdin E, Zhou MM. Structural basis of lysine-acetylated HIV-1 Tat recognition by PCAF bromodomain. Mol Cell 2002;9:575–586.
22. Tamkun JW, Deuring R, Scott MP, Kissinger M, Pattatucci AM, Kaufman TC, Kennison JA. Brahma: a regulator of *Drosophila* homeotic genes structurally related to the yeast transcriptional activator SNF2/SWI2. Cell 1992;68:561–572.
23. Dhalluin C, Carlson JE, Zeng L, He C, Aggarwal AK, Zhou MM. Structure and ligand of a histone acetyltransferase bromodomain. Nature 1999;399:491–496.
24. Pantano S, Tyagi M, Giacca M, Carloni P. Amino acid modification in the HIV-1 Tat basic domain: insights from molecular dynamics and in vivo functional studies. J Mol Biol 2002;318:1331–1339.
25. Bayer P, Kraft M, Ejchart A, Westendorp M, Frank R, Rosch P. Structural studies of HIV-1 Tat protein. J Mol Biol 1995;247:529–535.
26. Wang W, Donini O, Reyes CM, Kollman PA. Biomolecular simulations: recent developments in force fields, simulations of enzyme catalysis, protein–ligand, protein–protein, and protein–nucleic acid noncovalent interactions. Annu Rev Biophys Biomol Struct 2001;30:211–243.
27. Pantano S, Tyagi M, Giacca M, Carloni P. Molecular dynamics simulations on HIV-1 Tat. Eur Biophys J 2004;33:344–351.
28. Smith DE, Deng L. Computer simulations of NaCl association in polarizable water. J Chem Phys 1994;100:3757–3766.
29. Darden TA, York D. Particle mesh Ewald: an N log(N) method for Ewald sums in large systems. J Chem Phys 1993;98:10089–10094.
30. Ryckaert JP, Ciccotti G, Berendsen HJC. Numerical integration of the Cartesian equations of motion of a system with constraints: molecular dynamics of n-alkanes. J Comput Phys 1977;23:327–341.
31. Berendsen HJC, Postma JPM, van Gunsteren WF, DiNola A,

Haak JR. Molecular dynamics with coupling to an external bath. J Chem Phys 1984;81:3684–3690.
32. Cornell WD, Cieplak P, Bayly CI. A second generation force field for the simulation of proteins, nucleic acids and organic molecules. J Am Chem Soc 1995;117:5179–5197.
33. Jorgensen WL, Chandrasekhar J, Madura JD. Comparison of simple potential functions for simulating liquid water. J Chem Phys 1983;79:926–935.
34. Tsui V, Case DA. Theory and applications of the generalized Born solvation model in macromolecular simulations. Biopolymers 2000; 56:275–291.
35. Connolly ML. Solvent-accessible surfaces of proteins and nucleic acids. Science 1983;221:709–713.
36. Hunenberger PH, Helms V, Narayana N, Taylor SS, McCammon JA. Determinants of ligand binding to cAMP-dependent protein kinase. Biochemistry 1999;38:2358–2366.
37. Rocchia W, Alexov E, Honig B. Extending the applicability of the Poisson–Boltzmann equation: multiple dielectric constant and multivalent ions. J Phys Chem B 2001;105:6507–6514.
38. Marcello A, Cinelli RA, Ferrari A, Signorelli A, Tyagi M, Pellegrini V, Beltram F, Giacca M. Visualization of in vivo direct interaction between HIV-1 Tat and human cyclin T1 in specific subcellular compartments by fluorescence resonance energy transfer. J Biol Chem 2001;276:39220–39225.
39. Marcello A, Ferrari A, Pellegrini V, Pegoraro G, Lusic M, Beltram F, Giacca M. Recruitment of human cyclin T1 to nuclear bodies through direct interaction with the PML protein. EMBO J 2003;22: 2156–2166.
40. Cara A, Cereseto A, Lori F, Reitz MS Jr. HIV-1 protein expression from synthetic circles of DNA mimicking the extrachromosomal forms of viral DNA. J Biol Chem 1996;271:5393–5397.
41. Owen DJ, Ornaghi P, Yang JC, Lowe N, Evans PR, Ballario P, Neuhaus D, Filetici P, Travers AA. The structural basis for the recognition of acetylated histone H4 by the bromodomain of histone acetyltransferase gcn5p. EMBO J 2000;19:6141–6149.
42. Mujtaba S, He Y, Zeng L, Yan S, Plotnikova O, Sachchidanand, Sanchez R, Zeleznik-Le NJ, Ronai Z, Zhou MM. Structural mechanism of the bromodomain of the coactivator CBP in p53 transcriptional activation. Mol Cell 2004;13:251–263.
43. Fernandez A, Scheraga HA. Insufficiently dehydrated hydrogen bonds as determinants of protein interactions. Proc Natl Acad Sci USA 2003;100:113–118.
44. Zeng L, Zhou MM. Bromodomain: an acetyl-lysine binding domain. FEBS Lett 2002;513:124–128.
45. Periasamy A, Day RN. Visualizing protein interactions in living cells using digitized GFP imaging and FRET microscopy. In: Sullivan KF, Kay SA, editors. Green fluorescent proteins: Vol. 58. Methods in cell biology. London: Academic Press; 1999. p 293–314.
46. Tsien RY, Miyawaki A. Seeing the machinery of live cells. Science 1998;280:1954–1955.
47. Heim R, Tsien RY. Engineering green fluorescent protein for improved brightness, longer wavelengths and fluorescence resonance energy transfer. Curr Biol 1996;6:178–182.
48. Day RN, Periasamy A, Schaufele F. Fluorescence resonance energy transfer microscopy of localized protein interactions in the living cell nucleus. Methods 2001;25:4–18.
49. Selvin PR. The renaissance of fluorescence resonance energy transfer. Nat Struct Biol 2000;7:730–734.
50. van Roessel P, Brand AH. Imaging into the future: visualizing gene expression and protein interactions with fluorescent proteins. Nat Cell Biol 2002;4:E15–E20.
51. Day RN. Visualization of Pit-1 transcription factor interactions in the living cell nucleus by fluorescence resonance energy transfer microscopy. Mol Endocrinol 1998;12:1410–1419.
52. Marcello A, Lusic M, Pegoraro G, Pellegrini V, Beltram F, Giacca M. Nuclear organization and the control of HIV-1 transcription. Gene 2004;326:1–11.
53. Bres V, Tagami H, Peloponese JM, Loret E, Jeang KT, Nakatani Y, Emiliani S, Benkirane M, Kiernan RE. Differential acetylation of Tat coordinates its interaction with the co-activators cyclin T1 and PCAF. EMBO J 2002;21:6811–6819.
54. Pantano S, Carloni P. Comparative analysis of HIV-1 Tat variants. Proteins 2005;58:638–643.
55. Liu Y, Wang Z, Rana TM. Visualizing a specific contact in the HIV-1 Tat protein fragment and *trans*-activation responsive region RNA complex by photocross-linking. J Biol Chem 1996;271: 10391–10396.
56. Kanno T, Kanno Y, Siegel RM, Jang MK, Lenardo MJ, Ozato K. Selective recognition of acetylated histones by bromodomain proteins visualized in living cells. Mol Cell 2004;13:33–43.